Model Validation of Loose Bolted Joints in Damaged Structural Systems

Jared Collins[1], Matt Nothnagel[2], Jake Pretko[3], Alan Barhorst, PhD.[4]

[1] Dept. of Mechanical Engineering, The University of Houston, Houston, TX 77204
[2] Dept. of Mechanical Engineering, Rose-Hulman Institute of Technology, Terre Haute, IN 47803
[3] Dept. of Mechanical Engineering, Virginia Commonwealth University, Richmond, VA 23220
[4] Dept. of Mechanical Engineering, Texas Tech University, Lubbock TX 79409-1021

NOMENCLATURE

I_{cm}	moment of inertia about the center of mass
I_o	moment of inertia located at the origin
m	mass
d	distance
I	Inertia
b	thickness
h	height
E	Modulus of Elasticity
¼n	natural frequency
¼	density
L	length
¼	strain
¼	tip deflection
c	distance to neutral axis
x	position of the strain patch on the beam

ABSTRACT

The bolted or riveted lap joint is a common fastening technology for structural members. When a joint becomes worn the connected members can move in a nonlinear fashion as well as impact each other and the lap joint plates. For low frequency bending modes the system can experience sticking or frictional sliding motion at the contact points. Proposed in this project is the experimental validation of a theoretical frictional contact-impact model of the typical loose bolted joint.

1 INTRODUCTION

The purpose of this work is to validate a low-order model of a loose bolted joint that should enable prediction of the dynamic behavior of the loose joint. In contrast to a typical bolted joint, this joint has been constructed to mimic a damaged or worn connection. Because macroscopic motion is allowed in the joint, it is far more complicated than a typical apparatus, and exhibits significant non-linear effects in some excitation regimes.

Although significant research has investigated the physics and dynamics of joint interactions, and the associated damping, much of it has little application to this experiment. Joint motion is typically characterized as one of two separate phenomena. The first is termed *microslip* and consists of small, localized movements that do not cause motion between the actual parts of the joint. At higher levels of force excitation, the entire contact area of the joint will be in motion, and this is termed *macroslip* [1]. Extensive research on the damping and energy dissipation in microslip conditions has been performed. Gaul and Lenz [2] performed experiments on a bolted single-lap joint under different loadings to study force-deflection relationships. Their research showed that under different loads, the systems exhibited two regions of energy dissipation; these were attributed to microslip and macroslip.

Goodman [3] has studied interfaces which experience localized slipping. According to his research, for a wide variety of joints, there exists a power law relationship between force input to the system and energy dissipated. Researchers at Sandia National Laboratories [4, 5] have performed further investigations to identify the physics at joint interfaces. Additional work has been done at Los Alamos National Labs by Moloney et al. into the characterization of damping in bolted lap joints [6] and by Kess et al. into the effects of the bearing surfaces on damping [7].

None of these experiments or investigations lend themselves to low-order models. At Sandia, a large finite element model with hundreds of thousands of degrees of freedom was constructed and determined to predict the physics of a joint with some degree of precision [8]. Such a model, however, is impractical for modeling a real structure, of which the joint composes a minor, but critical component. However, further work at Sandia has examined Iwan models [9] to describe joints [10]. Iwan models are based on parallel-series and series-parallel networks of springs and sliders. The slider elements exhibit the properties of Coulomb friction, and model some of the non-linearities encountered in movement interfaces. Analytic expressions for the stress-strain behavior of these networks were derived by Iwan in connection with his investigations into metal plasticity. However, these expressions are also applicable to joint dynamics. Using Iwan models, Hartwigsen, et al. [11] created a low-order model of a lap joint that, according to them, seemed capable of simulating the dynamics of a joint in a structure.

All of these investigations, however, model joints in a relatively tight, or undamaged, condition. This experiment is designed to validate a model of a loose, damaged joint, which experiences significantly more movement than any of the micro or macroslip studies already performed. The model under consideration uses a unique approach to simulating hybrid-parameter multiple-body systems that has been extensively developed by Barhorst [12-16]. In contrast to other models, the joint and beam system is modeled using only nine degrees of freedom, including large elastic motions. This allows for much faster calculation times, while maintaining sufficient accuracy to correctly predict the dynamic behavior of the joint. This paper includes a discussion of the model, the experimental configuration, the system parameter identification, and the results of the experimental validation of the simulation model. The suitability and uses of this modeling method for simulating joint behavior is also discussed.

2 MODELING AND SIMULATION

2.1 MODELING METHOD

The method used in modeling the behavior of the beam is based on a technique developed by Barhorst [12-16]. The technique is a hybrid parameter multiple body system (HPMBS) modeling technique based on the variational projection methods of Gibbs-Appell. Figure 1 shows the elastic model of the cantilever beam with loose joint and tip load. A stinger excites the system at a point 1/3 the length of the left-most beam as measured from the base. Large displacements in the elastic members are indicated. The rigid joint model is depicted in Figure 2. Here the model assumes the contact can occur at four distinct points in and on the joint, see Figure 4. Double point contacts can occur. Three discrete coordinates are used to model the motion in the joint.

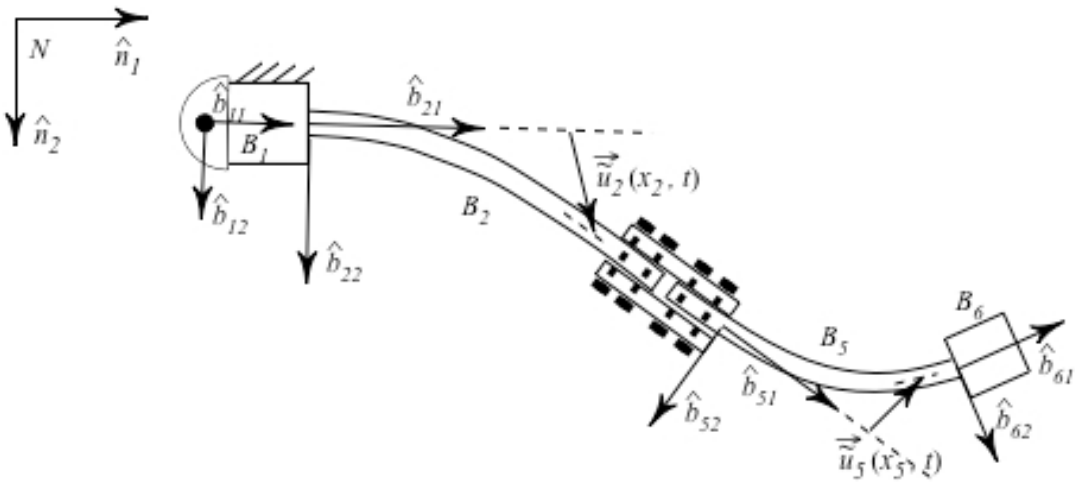

Figure 1: Cantilever Beam with Loose Bolted Joint

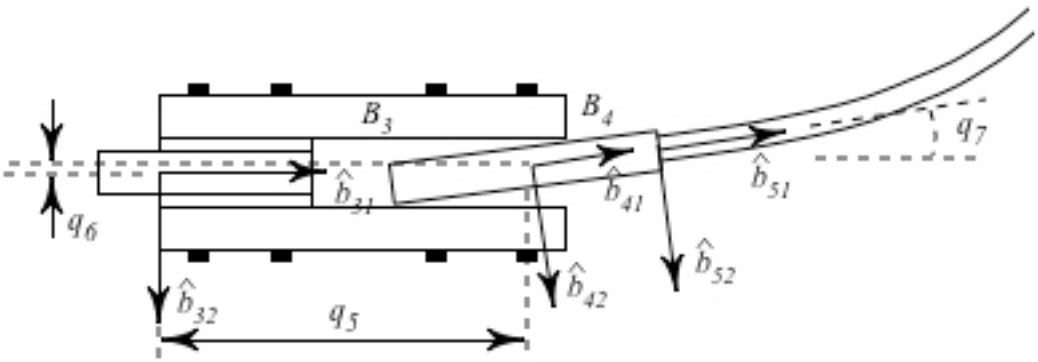

Figure 2: Loose Joint Details

The contact constraint dynamics are implemented with the idea of instantly applied non-holonomic constraints and thus the system model is of variable structure. If a single point is in slipping contact then the system order drops by a single degree of freedom. If the system is sticking at a single point then two degrees of freedom are lost, etc. This type of constraint implementation results in 17 distinct motion regimes combining the point(s) in contact as well as the motion regimes of either sticking or slipping at a given contact point.

In order to transfer the momentum exchanged during the switching dynamics described above, generalized momentum equations for HPMBS are utilized. Again the idea of instantly applied non-holonomic constraints allows the momenta to be funneled to the lower order system dynamics when a new contact point or motion regime (stick/slip) occurs. This allows 54 sets of momentum transfer equations to be written for the system at hand. It should be noted that the contact equations do not rely on penalty methods or coefficients of restitution.

The equations for numerical simulation are formulated via the variational weakening of the field equations of motion as well as the momentum transfer equations. Hermite polynomials are the functions used to describe the deflection and elongation fields of each beam. Three discrete generalized coordinates are use to parameterize the time bases of the elastic fields for each beam. The maximum number of degrees of freedom for the system is 9; there are also 9 kinematic differential equations for a total system order of 18 when the system is not in contact

at any points; this number decreases or increases as the constraints come into and out of play, respectively, as described above.

2.2 MODEL SYSTEM PARAMETERS

In order to create a low order model of a loose bolted joint, the system was separated into different sections, of which each component has several system parameters that need to be determined in order for the model to run. This section provides information about the various system parameters needed for the model to run. How the system parameters were identified will be discussed in a later section.

Parameters such as length, mass, inertia, stiffness, and sensor location remained constant throughout the experiment. The constant parameter values are located in various tables. Other parameters varied based on the type of test performed. Several test-dependent parameters include frequency, amplitude, gap width, damping estimates, simulation time, and initial conditions.

2.3 SIMULATION

To model the behavior of the joint the simulation outputs position, velocity, acceleration, strain, and points of contact in the joint. In order to validate the model, experimental data will be compared to simulation data at points corresponding to sensors located on the beam.

After the system parameters are loaded, the simulation algorithm begins by initializing the contact regime in a free state in which no points are touching. The algorithm then enters a loop that depends on the initial time step being less then or equal to the final time step. Within the loop, the velocity and position of the possible points of contact in the joint are calculated. The sign of the velocity determines whether or not the point is approaching contact. The position of each contact point is compared to an input parameter of the system. The position must be equal to the input parameter and the velocity must be in the correct direction for the algorithm to register contact in the joint. If no contact is made, an ordinary differential equation solver, LSODA, solves the equations of motion for a free flight situation. Strain and acceleration are then calculated and the initial time step is incremented. If the algorithm determines contact has occurred, one of nine different regimes corresponding to the nine possible cases in which contact occurs is called to determine if the contact is in a slip or stick condition. If the regime returns an odd number the contact at that point is sticking and if the regime returns an even number the contact is slipping. The LSODA integrator is then called to solve the equations of motion for the particular situation. The strain and acceleration are then calculated and the initial time step incremented. The loop continues updating the position of the contact points at each time step, determining what point or points are in contact, solving the equations of motion for the particular case, calculating strain and acceleration, and incrementing the initial time step until it is equal to the final time step.

3 EXPERIMENTAL TEST BED

3.1 PHYSICAL BEAM

The apparatus being studied consists of two flexible beams, a loose bolted joint, and a detachable tip mass. The entire system is comprised of aluminum components attached with steel bolts and nylon lock nuts. Since the model does not take into account impact due to sliding in the joint, cork filler is used to dampen these effects.

Assembly of the beam consists of cantilevering one of the flexible components, then attaching plates to the free end with steel bolts and lock nuts to create the first half of the joint. The gap in the joint is determined by placing feeler gauges between the interface of the plates and the flexible component. Cork filler is placed in the slotted section of the second flexible beam before it is attached to the joint in order to help dampen the nonlinear effects of contact in the joint due to sliding. The second flexible beam is then attached to the joint using bolts and lock nuts, but this time with a gap to form a loose joint. The gap is created by placing feeler gauges between the bolts in the second beam, then, after tightening, removing them. The free end is reserved for a tip mass of 152 grams that can be detached easily for testing purposes. The joint dimensions can be seen in Figure 3.

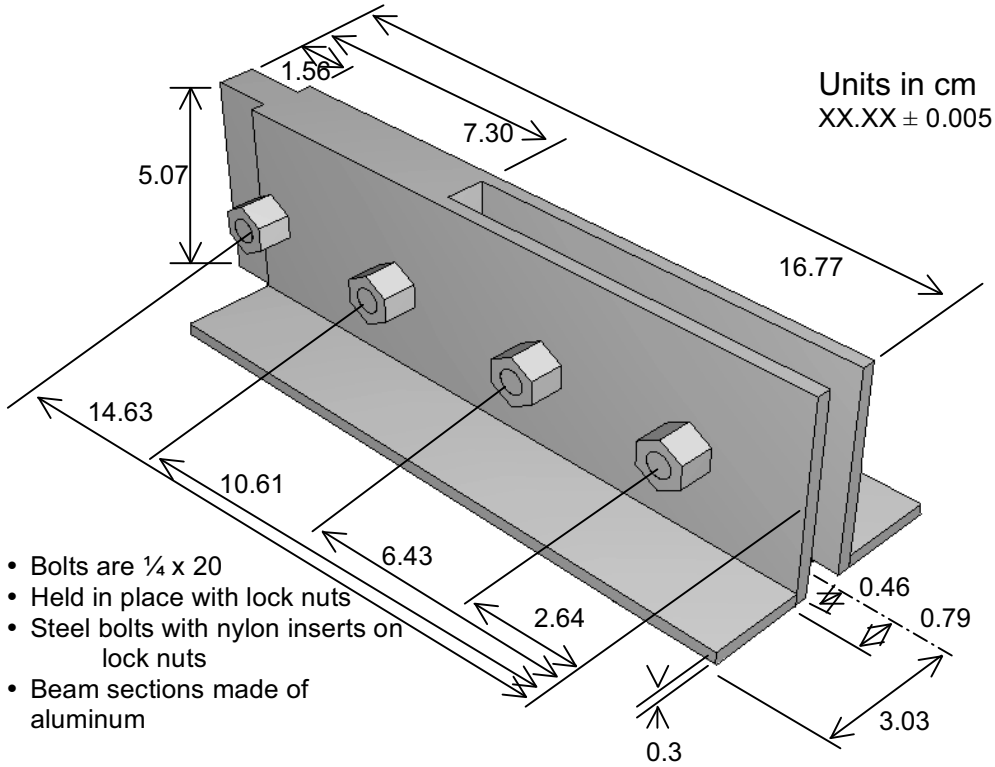

Figure 3: Dimensioned Joint

3.2 SENSORS

The sensors used for the experimental set-up of the loose bolted joint consist of one force transducer, three accelerometers, two strain gauges, and four contact sensors. The sensor, manufacturer, and model number of the sensors used in the experiment are displayed in Table 1. To describe the location of the ten sensors the same technique of dividing the beam into six separate sections, as discussed in section 2.2, will be used as reference.

Table 1

Sensor	Manufacturer	Model Number
Accelerometer	PCB Piezotronics	352A24
Strain Gauges	Measurement Specialties Inc.	DT1-052 K/W/TH
Force Transducer	PCB Piezotronics	208C03
Contact Patches	Measurement Specialties Inc.	DT1-052 K/W/TH

Each sensor is named based on the type of sensor and its location relative to the origin. The origin of the beam is taken to be at the cantilevered end and numbering of each sensor increases with distance from the origin. For example, the strain gauge closest to the origin is strain1 and the accelerometer farthest from the origin is accel3. The naming scheme for the contact sensors differs in the fact that two sets of contact patches are at the same distance from the origin. The figure below, Figure 4, illustrates the numbering scheme for the contact patches.

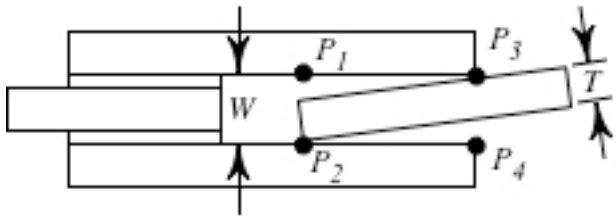

Figure 4: Contact Points

Figure 4 is a simplified diagram of the top view of the loose joint. The cantilevered end is located on the left and the free end is located on the right of the figure. The points corresponding to 1, 2, 3, and 4 are contact sensor locations. The contact patch located at 1 in the figure corresponds to contact1 and the contact patch located at 4 corresponds to contact4.

Table 2 contains the sensor name, the section the sensor is located, and the distance from the sensor to the end of the section that is closest to the origin.

Table 2

Sensor	Section	Distance (cm)
Force1	2	13.2
Strain1	2	21.9
Accel1	3	4.4
Contact1	3	8.3
Contact2	3	8.3
Contact3	3	14.5
Contact4	3	14.5
Accel2	4	10.5
Strain2	5	13.4
Accel3	5	28.4

3.3 EXCITATION AND DATA COLLECTION

All experimental data was collected utilizing a National Instruments PXI – 1042Q chassis with three of the eight cards utilized. A Labworks Inc. Model ET-132-2 Electrodynamic Shaker or a PCB Piezotronics Model 086C03 Impact hammer provided excitation for the different experiments conducted. The different tests and procedures will be discussed in a latter section.

3.4 SOFTWARE SET-UP

For each of the four tests performed, a virtual instrument is written in LabVIEW that collects the data and creates a tab-delimited text output file that is used for analysis in MATLAB. Each of the four virtual instruments are inherently similar, allowing the user to select a number of options depending on the test performed, such as amplitudes and frequencies sent out to the shaker. Figure 5 shows the user interface for the sine chirp test. As can be seen, the user may select the amplitude, start frequency, and end frequency, as well as the duration of the test. The graphs seen to the right of the control knobs display the data collected during the test.

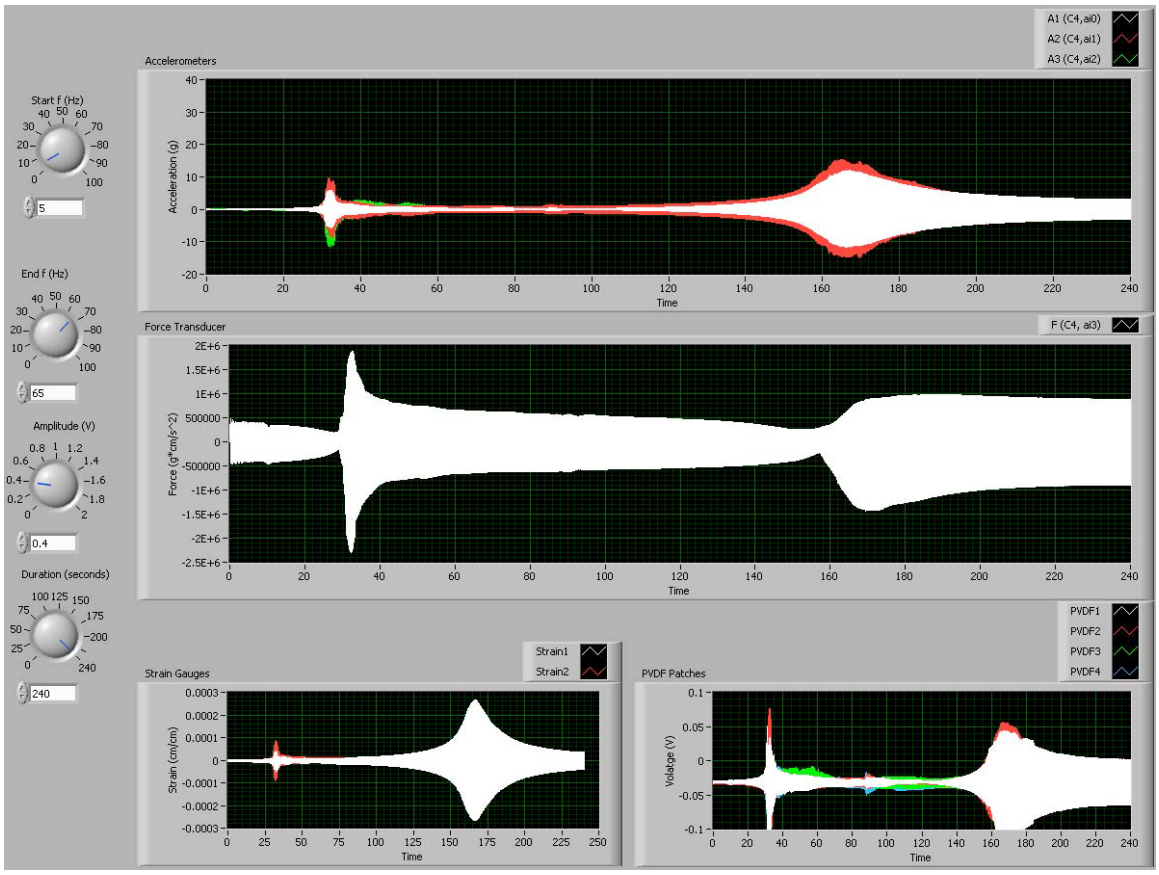

Figure 5: Chirp User Interface

3.5 CONTACT DETECTION

Four PVDF patches were installed inside the joint to act as contact sensors for the experiment. Each patch is installed along the outer joint plates so that when assembled, the edge of the loose beam is approximately mid-way across the patch. When in motion, the beam should contact the patch and compress it. This will produce a voltage that is recorded by the data acquisition system. All four sensors are recorded and written to a file for later analysis in MATLAB.

The MATLAB algorithm that was written to detect contact works by searching for peak values in the voltage above a predefined threshold. The algorithm creates a vector with the time of each peak value, and then combines the four vectors, one for each sensor, into a master vector that contains the type of contact at each point. By design it only searches for a maximum of two points in contact, similar to the model. The output is then a graph with time as the independent variable and contact on the dependant axis, where 1, 2, 3, or 4 represent contact at each point, respectively; and similar two digit numbers are assigned to the possible dual point contacts.

4 PARAMETER IDENTIFICATION

4.1 MASS

To determine the mass of the three rigid bodies, models of each body were generated using the finite element analysis software ABAQUS. Part of the preprocessing in an Explicit Dynamic simulation is a mass calculation. The mass provided by the ABAQUS model was confirmed by weighing detachable parts of the rigid bodies on a gram scale and estimating the mass of parts that were not able to be weighed by using the density of the material. The density of the material was determined by weighing a sample piece of the material on a gram scale and dividing the mass by the volume of the object. Another parameter that needed to be identified for input into the model was the mass per unit length of the two elastic bodies. The mass per unit length of the two rigid bodies were determined by dividing the mass determined by the gram scale by the length of the elastic section. Located

in Table 3 is the density of the aluminum beam, mass of the rigid bodies, and the mass per unit length of the elastic bodies.

Table 3

Density	2.5065 g/cm3
Rigid Sections	Mass (g)
3	313.81
4	123.33
6	158.9
Elastic bodies	Mass/length (g/cm)
2	4.0428
5	4.0428

4.2 INERTIA

To determine the mass moment of inertia of the three rigid bodies, models of each body were generated using the finite element analysis software ABAQUS. Part of the preprocessing in an Explicit Dynamic simulation is a mass moment of inertia calculation. The moment of inertia about the center of mass (I_{cm}) for Section-3 of the beam in the direction relevant to the simulation was determined to be 6973.4 gcm^2. For input into the model, the moment of inertia had to be located at the origin of Section-3 in the model.

$I_o = I_{cm} + md^2$

The above equation was used to determine the mass moment of inertia at the origin (I_o). The mass of the section (m) is provided in Table 3 and the distance (d) from the center of mass to the origin is 7.559 cm. The origin of Section-4 and Section-6 are at the center of mass of the part, therefore, values for the moment of inertia are taken directly from ABAQUS. The inertia per unit length was determined by multiplying the density from Table 3 by the inertia (I) determined by the equation below.

$$I = \frac{1}{12} bh^3 \tag{1}$$

In the above equation, b is the thickness of the beam and h is the height of the beam. Below, in Table 4, is all inertia and inertia per unit length values that were determined for the input into the simulation.

Table 4

Rigid Sections	Inertia (gcm^2)
3	24904
4	1398.60
6	301.55
Elastic Sections	Inertia/length (g/cm)
2	0.03396
5	0.03396

4.3 CORK CHARACTERISTICS

As was previously stated in the theory and model section of this paper, the simulation does not model impacts between the bolts on the loose beam and the slot joints in the rigid body of the joint. To enforce this condition, small pieces of cork filler were used to pad the outside of the slotted joints. To capture these effects in the simulation, the stiffness and damping properties need to be known.

Two separate methods were used to find parameters. The first was a static compression used to find stiffness. The beam, in its assembled form, was compressed with a known force measured using a scale. The gap between the fixed beam and the loose beam inside the joint was measured prior to the load application and during the application. By comparing the force to the deflection, we can use Hooke's law to find the spring constant. Table 5 below summarizes the results of three such trials.

Table 5

Applied Load (g*cm/s^2)	Pre-Load Gap (cm)	Load Gap (cm)	Stiffness (g/s^2)
3.14E+06	0.71	0.635	4.19E+07
4.12E+06	0.77	0.585	2.23E+07
3.92E+06	0.635	0.58	7.13E+07

The second method was to instrument the end of the system with an accelerometer mounted on the tip mass in the axial direction. The beam was then impacted on the end with a hammer, and the damped oscillation was recorded with the accelerometer. An exhaustive search algorithm was written in MATLAB to try different combinations of initial velocity, stiffness, and damping. The fitness of each combination was judged based a squared difference between the model and the accelerometer data. The best fit value was saved and output by the algorithm. In addition to the typical linear relationship between displacement and spring force, both a quadratic and cubic model were tested, when the spring force is proportional to the displacement squared and cubed, respectively. The table below details the best results from the different simulations.

Table 6

Test	Stiffness (g/s^2)	Damping (g/s)
DE-1	2.70E+05	1.10E+04
DE-2	2.70E+05	9.50E+03
DE-3	4.83E+05	1.75E+04
DE-K~x^2	(g/(s^2*cm)) 6.00E+04	2.00E+04
DE-K~x^3	(g/(s^2*cm^2)) 1.00E+04	2.20E+04

In our simulations, the best agreement came when using the cubic stiffness model, so that is the value currently implemented. For the damping value, we are using an average of the different values found, 1.7e4 g/s.

4.4 MODULUS OF ELASTICITY CALCULATION

In order to find the modulus of elasticity in the aluminum members that comprise the joint, logarithmic decrement is performed on data collected from a special setup. In this system, the flexible bodies in the beam are separated from the main apparatus and cantilevered. A deflection, ¼ of about 2.70 cm is applied to the beam and then released, with acceleration data collected and output to a text file. This is performed three times. Damping ratios are then tabulated in order to find the natural frequency of the beam, and the following equation, derived in appendix A, is used to calculate the modulus of elasticity, E:

$$E = \frac{11\rho_n^2 \rho L^4}{140 I} \tag{2}$$

Where:

- E = Modulus of Elasticity ($\frac{g}{cm * s^2}$)
- I = Moment of Inertia (cm^4)
- ¼$_n$ = Natural Frequency (rad/s)
- ¼= Linear density of material (g/cm)

- L = Length of beam (cm)

The results of these calculations can be found in Appendix B. To find the natural frequency, equations from Ogata's textbook are used. The computed average moduli of elasticity for the first and second are 50.48 GPa and 46.12 GPa, respectively. These values are input into the simulation to help predict the response of the assembled beam. In the end the standard values for these parameters were used in the simulations.

4.4 STRAIN SENSOR PATCH CALIBRATION

In the absence of strain gauges, PVDF patches are used as both contact detectors and strain sensors. Since the contact sensors only rely on the timing of the signal, no calibration is required, however, the strain patches need to be calibrated. To complete this task, the two flexible parts of the beam that actually have the strain patches attached are taken off of the apparatus and cantilevered. A static deflection is then applied and released, and the data is collected. To assist calibration, an accelerometer is placed on the end of the cantilevered beam. The acceleration data is then numerically integrated twice using Euler's method of approximation and then transformed into strain using the following equation, which is derived in Appendix C:

$$\varepsilon = \frac{3\delta_L c}{L^2}\left(\frac{x}{L} - 1\right) \tag{3}$$

Where:
- ε = Strain (cm/cm)
- δ_L = Tip deflection (cm)
- c = Distance to neutral axis (cm)
- x = Position of the strain patch on the beam (cm)
- L = Length of the beam (cm)

The converted acceleration data is then plotted with the strain data and a multiplier is found to give a scaling factor for use to extract strain from the voltage output by the PVDF patches. The multipliers for patch 1 and 2 were 9e-5 and 1.77e-5, respectively.

5 PROCEDURES

5.1 EXPERIENTAL TEST SETUP

To assist model validation, four gap widths were selected for the ends of the loose bolted joint, namely 0.508 mm, 0.635 mm, 0.762 mm, and 1.016 mm. These gaps were chosen to give a range of beam conditions simulating different damage levels. The beam is assembled with feeler gauges near the bolts to provide a consistent gap width in the apparatus. The sensors are then attached to the beam in their respective places. It is then tested under four excitation conditions, namely deflection, chirp, impulse, and shaker inputs. Each testing method has its own virtual instrument associated with it, written in LabVIEW.

5.2 SHAKER EXCITATION

To test the response of the beam to a sine wave excitation, a Model ET-132-2 & -203 shaker and amplifier combination are utilized to stimulate the beam at frequencies ranging from 10-55 Hz, in increments of 5 Hz. Frequencies outside of this range do not provide a measurable response with the equipment provided. Each frequency is tested using three trials both with and without the end mass attached to the beam, providing for a total number of six trials with each frequency. The amplitude for each shaker test is modified so as to not saturate the sensors, and tends to range from 0.4 to 0.8 volts. This amplitude is determined visually by running a short test and viewing the output graph to look for saturation trends. Once the frequency and amplitude is set for a given trial, the shaker excites the beam for a period of ten seconds, after which a LabVIEW Measurement File is written that includes all of the test data for future analysis. This data is then analyzed using MATLAB and compared to the predicted values from the simulation.

5.3 DEFLECTION EXCITATION

To test the free response of the system, the shaker and force transducer are detached and a static deflection of 8.4 cm is applied to the free end of the beam. This deflection is selected because it is slightly higher than the deflections seen in shaker tests. When released, a LabVIEW virtual instrument records the sensor data for a period of twenty seconds, after which it writes out a measurement file in the form of a tab-delimited text file for both analysis purposes and helping determine damping characteristics. The deflections are repeated three times each, both with and without the tip mass attached.

5.4 IMPULSE EXCITATION

To test the free response of the system to an impulse, the force transducer and the shaker are detached and an impact hammer is used to excite the system at the base of the third member. The impulse force as well as the sensor data is collected using a LabVIEW virtual instrument that collects the information over a period of ten seconds, after which it writes out a tab delimited text data file. This data helps determine damping characteristics in the joint that can be used in the simulation.

5.5 CHIRP EXCITATION

To test the response of the system to a chirp excitation (a constant ramping between two frequencies), a special LabVIEW virtual instrument was written that creates a chirp based on the user's specifications for frequency, amplitude, and duration. The simulation is run for a period of four minutes to allow sufficient time for transients to subside in the response of the beam. This is repeated three times for each gap width in a frequency band of 5-65 Hz. Once the information is collected, LabVIEW creates a tab delimited data file that is used to compare the actual response with what is predicted in the model.

6 DATA COMPARISON AND RESULTS

For the actual model validation, several different types of data were compared. They fall into four categories. The simplest method of comparison is the visual inspection of time-domain data from simulations and experiments. An example of this is included here as Figure 6.

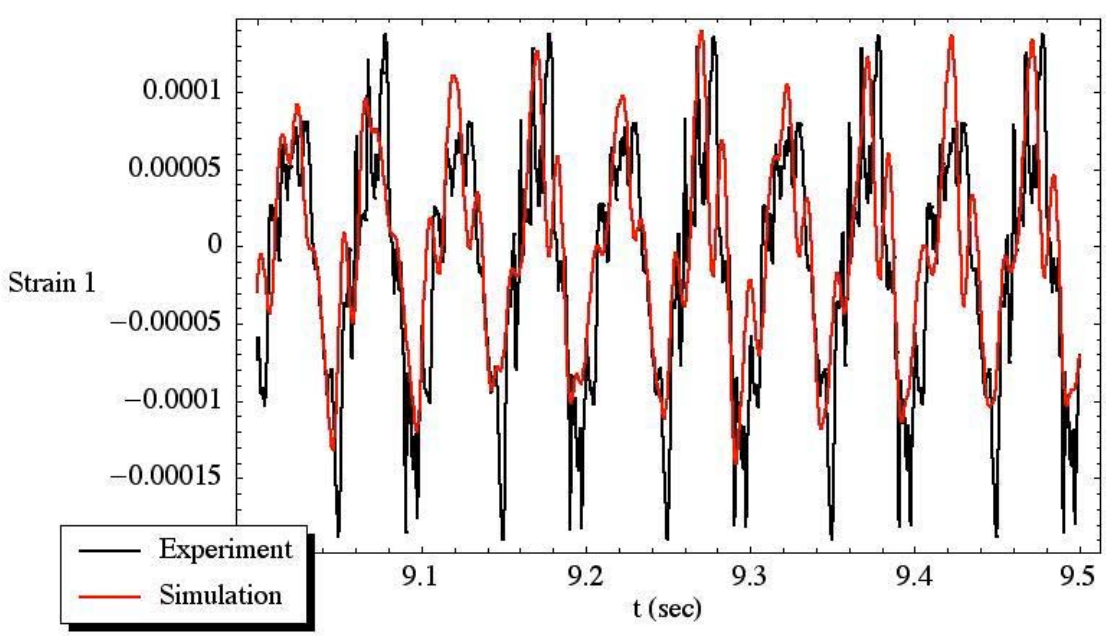

Figure 6: Time Domain Comparison of Simulation with Experiment

This is a direct comparison of a portion of the output from a simulation and experiment with a 1.016 mm gap width run with a constant amplitude shaker input at 20 Hz for 10 seconds. Although it is not an exact match for the experiment, the simulation is showing a strong resemblance to the recorded data. Both the main driving frequency and signal amplitudes match well. Similar comparisons of the accelerometer data, as well as the other strain gauges can be made.

The second method of comparison is to take the time-domain data previously mentioned and use a fast Fourier transform on it to determine the frequency content of the signals. Figures 7 and 8 are plots of the signal content of strain gauge 2 under the same conditions in experiment and simulation.

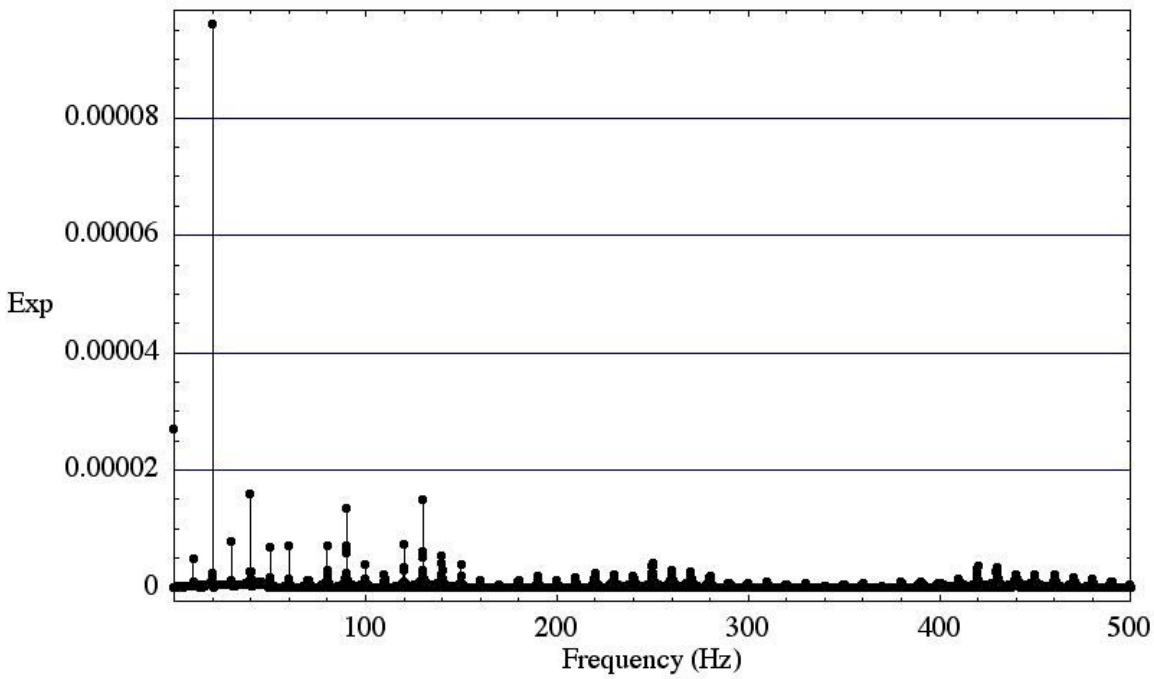

Figure 7: Strain1-Experimental Power Spectrum

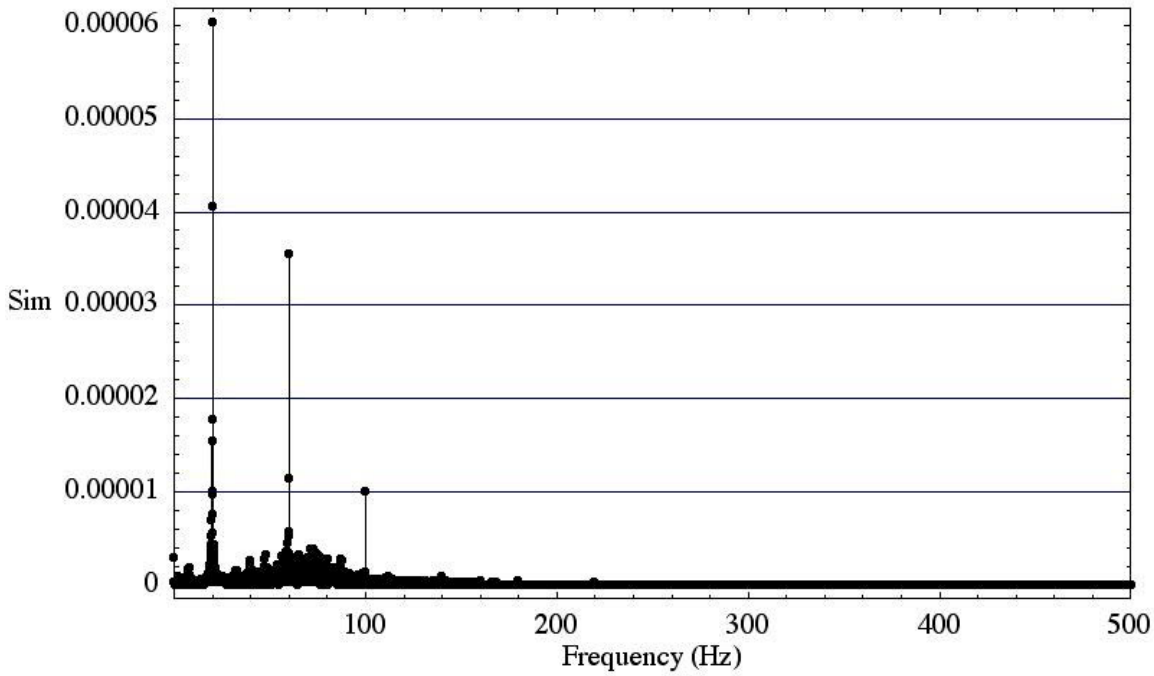

Figure 8: Strain 1-Simulation Power Spectrum

While the driving frequency stands out very well, and some of the other frequencies as well, this match is not as good as the previous time-domain data. Some features do match, such as the sub harmonic at 10 Hz, and there are similarities between the higher frequency peaks around 60 and 100 Hz. However, the frequencies are not exact, as they are shifted a bit higher than the experiment, and none of the information above 200 Hz is really present in the simulation. The simulation is also showing more energy at peaks other than the driving frequency, whereas all of the energy in the experiment is concentrated there. The other data has similar trends. There are some promising points in these data comparisons, but they need further investigation.

The third standard method of data comparison is for the contact behavior in the joint. The simulation outputs a contact diagram as a part of the simulation (Figure 9), and experimental data (Figure 10) comes from the PVDF patches attached to the joint, and processed by a MATLAB script written for this purpose.

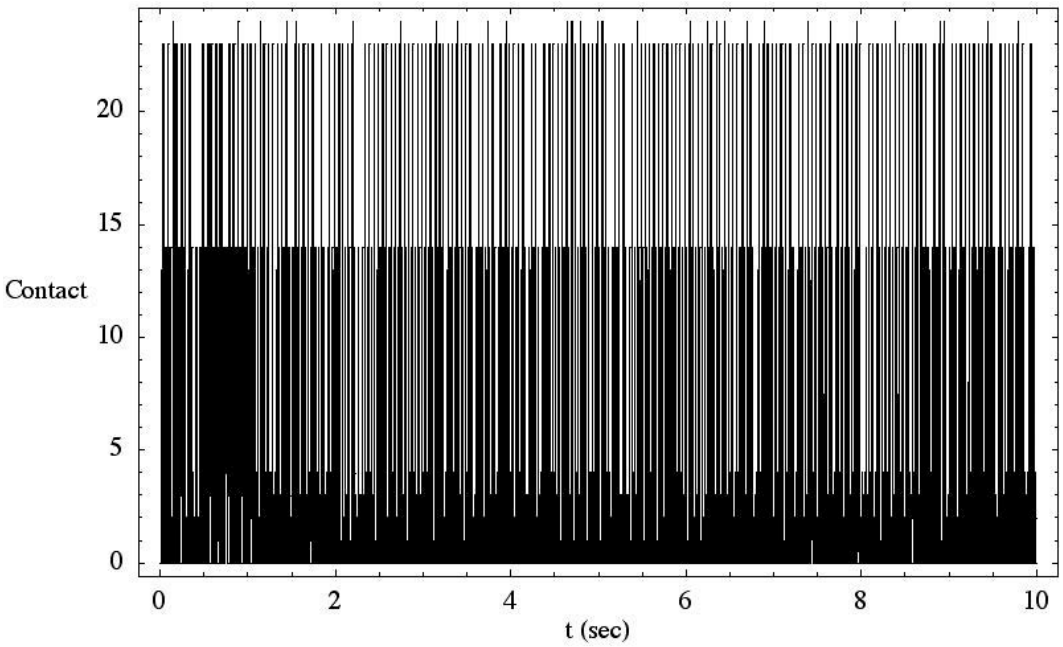

Figure 9: Simulation Contact Point Switching

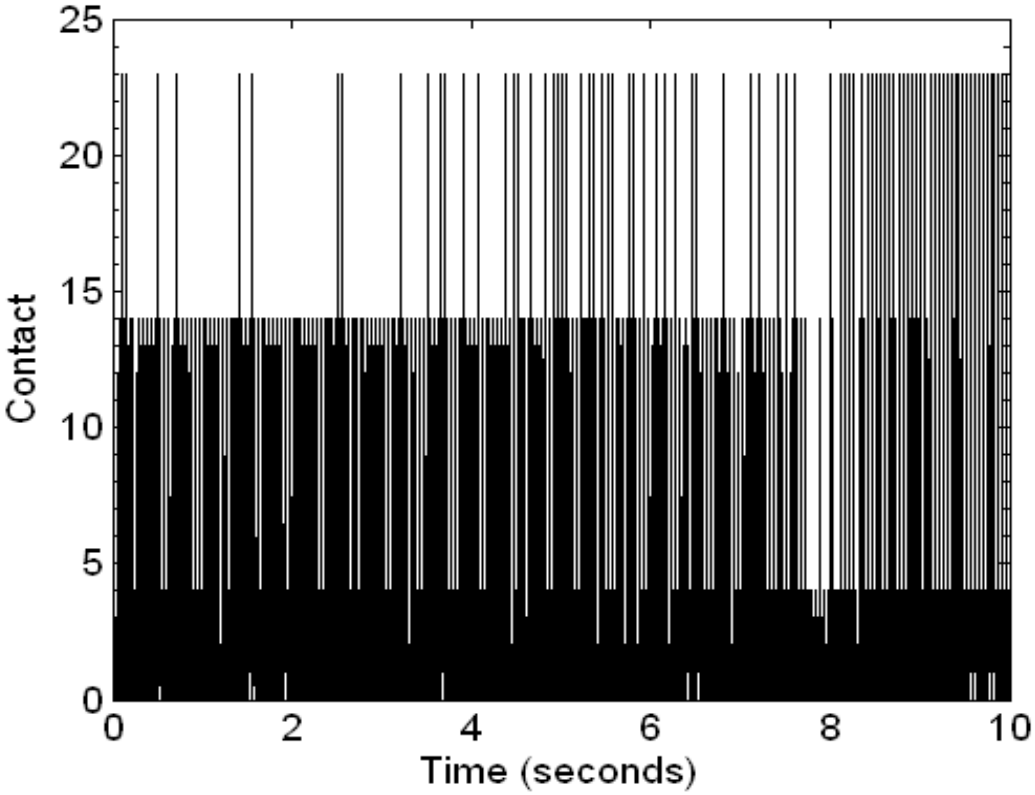

Figure 10: Experiment Contact Point Switching

These contact diagrams show some similarities. The vertical axis refers to the point in contact at that time. For two digit numbers, this is the combination of points in contact at that time. The top diagram, from the simulation, is showing a lot of switching from contact at 1 and 4 to contact at 2 and 3 (see Figure 4). Similarly, the bottom diagram, for the experiment, is showing a lot of contact between the same sets of points, in addition to contact at 1 and 3. The match is not perfect, as there seems to be a difference in the frequency of switches between each

contact regime between the simulation and the experiment, but because the same sorts of patterns are showing up in the switches, it provides some confidence that the behavior is being model with some accuracy.

The final method of comparison is only relevant for the sine chirp experiments. Instead of attempting to compare the time-domain values, we are more interested in the bands of frequency where the beam is in a region of resonance. To find these areas, a short-time Fourier transform is used to get frequency content at many points in time. The result is plotted as a spectrogram (Figures 11 and 12), and by comparing regions of elevated activity. The spectrograms are from a Sine chirp done from 5 Hz to 65 Hz, over the course of four minutes. Features of interest have been boxed, and will be explained below.

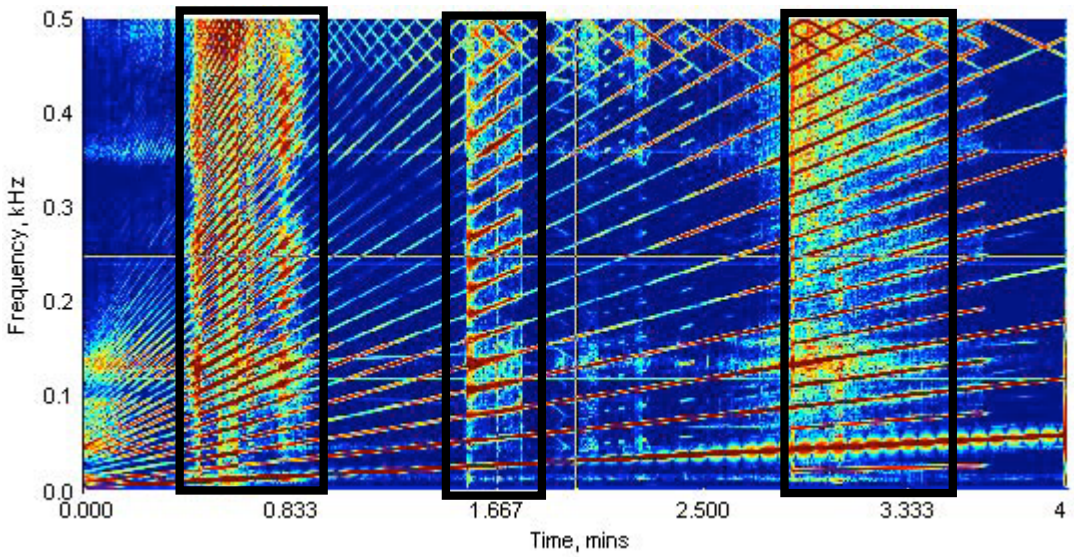

Figure 3: Experiment Spectrogram

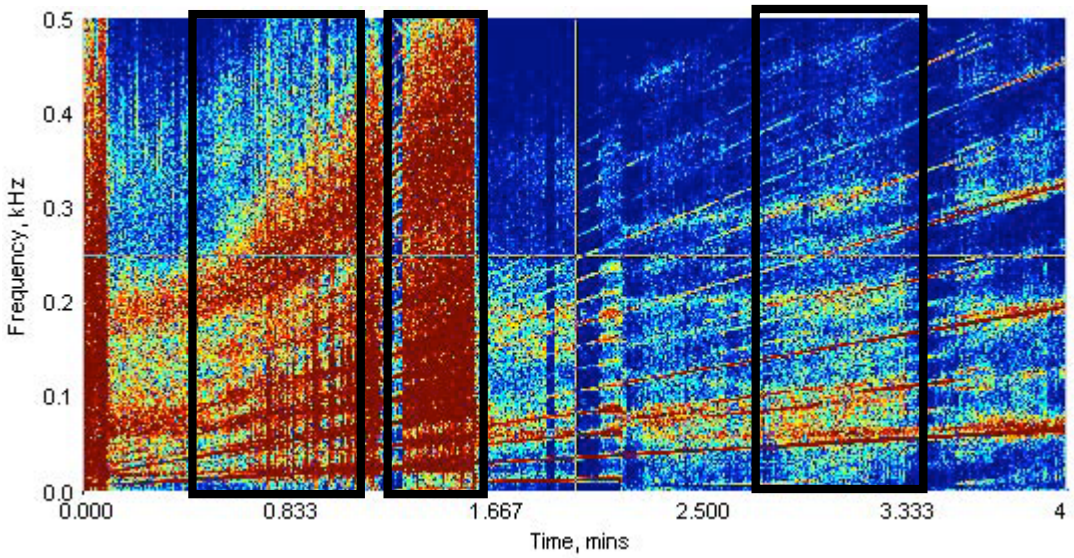

Figure 12: Simulation Spectrogram

The driving frequency and its integer multiples are visible as diagonal bands of dark red starting in the lower left corner and propagating right and up across the charts. The first several seconds of the simulation (Figure 12) should be ignored, as the system is overrun with transient behavior that appears to have little relevance. However, there do appear to be several matching bands of excitation in the charts. The first main band in the experiment (Figure 11), around 0.83 minutes appears to be showing up slightly later in the simulation. The next

band appears around 1.667 minutes in the experiment, and shows some correlation with the simulation band just prior to the same time. The final band at around 3 minutes is more problematic in that it is more spread out; however, it may be related to the increased excitation at about the same time in the simulation. Overall, there are encouraging trends in the chirp data; however time has not permitted us to run many of these simulations as they are computationally intensive.

7 CONCLUSIONS AND FUTURE WORK

7.1 CONCLUSIONS

The modeling of joints in a structure is becoming increasingly important as simulations become more and more accurate. However, given a relative lack of understanding of joint dynamics and first-principle physics, joints can either be quickly modeled inaccurately, or with many degrees of freedom, at the expense of computational speed. Additionally, while some investigations have been performed into the physics at the joint level in certain configurations, no research has been done on joints that simulated damaged conditions. This paper has examined the validity of using a Gibbs-Appell based approach to modeling joint dynamics using path formulations of the equations of motion to simplify the system under consideration. This offers a low order model with fewer than ten degrees of freedom that should accurately simulate the behavior, both in the time domain and in the frequency domain, of the joint.

The data generated by the simulation has been compared to experimental data, and shows promising results. Although some of the frequencies appear to be shifted either up or down from the experimental data, this is likely attributable to difficulties in finding the appropriate system parameters for the model. With future work, it should be possible to get good agreement between the simulation and reality, allowing for simulations of joints that are both fast and accurate.

7.2 FUTURE WORK

Numerous future plans have been developed to help expand the capabilities of the model. The most important idea is to create a parameter estimator to help find the correct inputs for use by the model. This algorithm would give information about the beam such as damping and elastic coefficients to help reduce the error in the simulation due to incorrect assumptions.

The next logical step for the model would be to modularize it for use in finite element analysis software. An algorithm that could be used in conjunction with finite element programs such as ABAQUS could prove quite useful by decreasing calculation times while trying to model a damaged structural system.

The logic associated with the model could also be utilized by a controller to mitigate damage. Many structures that use this type of joint can be found in locations that are either difficult or dangerous to repair. In this case, the controller could help mitigate damage propagation by helping the system avoid vibration regimes that could severely harm it.

Finally, modeling the joint as an elastic body would help the simulation predict experimental results more accurately. Representing the joint in this way would allow the simulation to predict the contact regimes that were seen in the experiments that are impossible given the assumption of a joint comprised of rigid bodies.

ACKNOWLEDGMENT

Funding for the Los Alamos Dynamics Summer School was provided by the Engineering Science and Applications Division at the Los Alamos National Laboratory and the Department of Energy's Critical Skills Programs Office. The following companies generously provided various software packages that were necessary to complete the student projects: Vibrant Technologies (experimental modal analysis software), The Mathworks, Inc. (numerical analysis software), and Hibbitt, Karlsson and Sorensen, Inc. (ABAQUS finite element software).

References

[1] M. Groper, Microslip and macroslip in bolted joints, *Experimental Mechanics* 25 (1985) 171-174

[2] L. Gaul, J. Lenz, Nonlinear dynamics of structures assembled by bolted joints, *Acta Mechanica* 125 (1997) 169-181.

[3] L.E. Goodman, A review of progress in analysis of interfacial slip damping, in: *Structural Damping, Proceedings of the American Society of Mechanical Engineers Annual Meeting*, Atlantic City, 1959, pp. 35-48.

[4] D.L. Gregory, D.O. Smallwood, R.G. Coleman, M.A. Nusser, Experimental studies to investigate damping in frictional shear joints, in: *Proceedings of 70th Shock and Vibration Symposium*, 1999.

[5] D.O. Smallwood, D.L. Gregory, R.G. Coleman, Damping investigations of a simplified frictional shear joint, in: *Proceedings of 71st Shock and Vibration Symposium*, 2000.

[6] C. W. Moloney , D. M. Peairs, E. R. Roldan, Characterization of Damping in Bolted Lap Joints, in: *Proceedings of International Modal Analysis Conference*, Kissimmee, FL, 2001.

[7] H. R. Kess, N. J. Rosnow, B. C. Sidle, Effects of Bearing Surfaces on Lap Joint Energy Dissipation, in: *Proceedings of International Modal Analysis Conference*, Los Angeles, CA, 2002.

[8] D.W. Lobitz, D.L. Gregory, D.O. Smallwood, Comparison of finite element predictions to measurements from the Sandia microslip experiment, in: *Proceedings of International Modal Analysis Conference*, Orlando, FL, 2001.

[9] W.D. Iwan, On a class of models for the yielding behavior of continuous and composite systems, *Journal of Applied Mechanics* 89 (1967) 612–617.

[10] D.J. Segalman, An initial overview of Iwan modeling for mechanical joints, Report SAND 2001-0811, Sandia National Laboratories, Albuquerque, NM, 2001.

[11] C.J. Hartwigsen, Y. Song, D.M. McFarland, L.A. Bergman, A.F. Vakakis, Experimental study of non-linear effects in a typical shear lap joint configuration, *Journal of Sound and Vibration* 227 (2004) 327-351.

[12] A. A. Barhorst, L. J. Everett, Modeling hybrid parameter multiple body systems: A different approach, *The International Journal of Nonlinear Mechanics* 30(1) (1995) 1-21.

[13] A. A. Barhorst, Systematic closed form modeling of hybrid parameter multiple body systems, *The International Journal of Nonlinear Mechanics* 39(1), (2004) 63-78

[14] A. A. Barhorst, On the efficacy of pseudo-coordinates – Part 1: Moving interior constraints, *The International Journal of Nonlinear Mechanics*, 39(1), (2004) 123-135

[15] A. A. Barhorst, On the efficacy of pseudo-coordinates – Part 2: Moving boundary constraints, *The International Journal of Nonlinear Mechanics*, 39(1), (2004) 137-151

[16] A. A. Barhorst, An Elasto-Dynamic Model of a Slewing Beam with a Loose Bolted Lap Joint. To appear.

[17] Ogata K. (2003), “System Dynamics,” Prentice Hall, 4th ed.

Appendix A: Derivation of Modulus of Elasticity Calculation

- From beam formulas, we can see that

$$P = \frac{3EI}{L^3}\delta \quad \textbf{(A1)}$$

- The beam acts as a spring, so

$$P = k\delta \quad \textbf{(A2)}$$

$$\therefore k = \frac{3EI}{L^3} \quad \textbf{(A3)}$$

- If we find the natural frequency, we can find EI.

$$\omega = \sqrt{\frac{k}{m}} \quad \textbf{(A4)}$$

- Now, use the kinetic energy equation.

$$\frac{1}{2}m\dot{\int}_L^2 = \frac{1}{2}\int_0^L \int \left(du/dt\right)^2 dx \quad \textbf{(A5)}$$

- From the beam equations, it can be seen that

$$u = \frac{-_L x^2}{2L^3}(3L - x) \quad \textbf{(A6)}$$

$$-\ du/dt = \frac{x^2}{2L^3}(3L - x)\dot{-}_L \quad \textbf{(A7)}$$

- Plugging in to (A5), we get

$$\frac{1}{2}m\dot{\int}_L^2 = \frac{1}{2}\int_0^L \int \frac{\int x^2}{\int 2L^3}\left(3L\int x\right)\dot{\int}_L \frac{\int^2}{\int} dx \quad \textbf{(A8)}$$

$$\therefore m = \frac{33 \cdot L}{140} \quad \textbf{(A9)}$$

- Plugging in to (A4) and rearranging,

$$\boxed{E = \frac{11\rho_n^2 \rho L^4}{140I}}$$

Appendix B – Calculated values from MoE Calculation

	x_1 (V)	x_n (V)	t_1 (s)	t_n (s)	n	T_d (s)	ω	$ω_n$ (rad/s)	EI ($\frac{g*cm^3}{s^2}$)	E (GPa)*
Beam 1, Trial 1	0.4499	0.03836	0.536	3.238	47	0.057489	0.0085	109.298	$6.862*10^9$	50.65
Beam 1, Trial 2	0.284	0.03186	0.885	3.821	51	0.057569	0.006963	109.144	$6.843*10^9$	50.51
Beam 1, Trial 3	0.2653	0.02939	0.935	3.935	52	0.057692	0.006866	108.912	$6.814*10^9$	50.29
Beam 2, Trial 1	0.3773	0.02629	0.901	3.939	62	0.049	0.00695	128.231	$6.269*10^9$	46.27
Beam 2, Trial 2	0.325	0.01605	1.826	5.855	82	0.049134	0.00591	127.881	$6.235*10^9$	46.02
Beam 2, Trial 3	0.4444	0.02866	0.864	3.958	63	0.049111	0.007037	127.942	$6.241*10^9$	46.06

*Note: These values are much lower than as expected (70-79 GPa)

Appendix C: Derivation of Strain Equations

- From beam equations,

$$\delta_L = \frac{PL^3}{3EI} \qquad \textbf{(C1)}$$

and

$$-_x = -\frac{Px^2}{6EI}(3L - x) \qquad \textbf{(C2)}$$

$$\therefore \frac{P}{EI} = \frac{3\cdot_L}{L^3} \qquad \textbf{(C3)}$$

- Plugging into **(C2)**,

$$-_x = -\frac{-_L x^2}{2L^3}(3L - x) \qquad \textbf{(C4)}$$

$$- \frac{-^2-}{-x^2} = \frac{3-_L x}{2L^3} - \frac{3-_L}{L^2} \qquad \textbf{(C5)}$$

- Using the moment equation,

$$M = \frac{\rfloor^2 \rfloor}{\rfloor x^2}(EI) = \frac{3\rfloor_L EI}{L^2}\left\rfloor \frac{x}{L} \rfloor 1 \right\rfloor \qquad \textbf{(C6)}$$

- Therefore, the bending stress is:

$$\rfloor = \frac{Mc}{I} = \frac{3\rfloor_L Ec}{L^2}\rfloor \frac{x}{L} \rfloor 1 \rfloor \qquad \textbf{(C7)}$$

- And, finally, from Hooke's Law

$$\boxed{\rfloor = \frac{\rfloor}{E} = \frac{3\rfloor_L c}{L^2}\rfloor \frac{x}{L} \rfloor 1 \rfloor}$$